Comparison of the terahertz and optical characteristics of graphene and silicene nanoribbons utilizing first-principles approach

S. YAMACLI
Nuh Naci Yazgan University, Dept. of Electrical-Electronics Engineering, Kayseri, Turkey.

Optical applications of graphene and related two-dimensional materials are continuously taking interest. In this study, accurate first-principles simulations are utilized for obtaining the terahertz and optical characteristics of realistic graphene and silicene nanoribbons (GNRs and SiNRs). Density functional theory is used for calculating the electron density and then Kubo-Greenwood formalism is applied for the computation and comparison of the complex dielectric functions of equivalent GNR and SiNR samples, which are found to be consistent with the previous results in the literature. Frequency-dependent complex conductivities of the devices under consideration are also obtained. The surface plasmon polariton (SPP) wave propagation properties of GNR and SiNR samples are then interpreted and compared. The frequency-dependent conductivity data are also imported into a full-wave electromagnetic simulation tool and the characteristics of the GNR and SiNR samples are evaluated for use as nanostrip transmission lines. It is found out that GNRs seem to be more advantageous compared to equivalent SiNRs from both SPP wave transmission frequency range and higher conductivity viewpoints.

(Received August 19, 2015; accepted September 29, 2016)

Keywords: Silicene, Graphene, Nanoribbon, Optical, Terahertz

1. Introduction

Hexagonal crystal of single layer carbon, graphene, attracted interest from various branches of science and technology in recent years as a promising material thanks to its extraordinary physical and electrical properties such as high electrical and thermal conductivity, strong mechanical characteristics and peculiar optical response [1]. Graphene is originally a two-dimensional structure while effectively one-dimensional thin strips of graphene, called graphene nanoribbons (GNRs), also find wide application areas thanks to their sensitively controlled electronic characteristics by the atomic configuration at the edges. It is well-established that GNRs with zigzag edges show conductive behaviour in contrast to armchair edged GNRs which have band gaps dependent on their widths [2].

Microwave and optical frequency behaviour of graphene and GNRs is also an active research area owing to the interesting properties of these materials in these frequency ranges. An important property of graphene in microwave frequencies is that it shows nonlinear current-voltage characteristics enabling to build simple mixer applications by using only a piece of graphene monolayer [3]. On the other hand, frequency-dependent variations of the dielectric function or susceptibility tensor of materials are in fact the main parameters determining the high-frequency response. Hence, dielectric functions of graphene and GNRs are investigated widely in the literature using different approaches. In one of these studies, tight-binding calculations are utilized for obtaining the dielectric function of graphene [4]. Ab initio methods are also used for studying the high-frequency response of graphene as in [5] for doped graphene structures. Optical adsorption of graphene in two directions is calculated in [6]. Similar to these studies, the complex dielectric function of graphene is calculated by either tight-binding methods or density functional theory (DFT) simulations in [7]. Utilization of graphene as terahertz and optical patch antennas are investigated in [8] by taking these dielectric functions into consideration. Moreover, it is shown that the electrical size of these patches are much larger than their physical dimensions enabling practical terahertz and optical antennas thanks to the surface plasmon polariton (SPP) waves in graphene patches [9]. Similarly, in [10], the dielectric function of very thin (N=7) GNRs are obtained by first-principles calculations. Jornet and Akyildiz have done a comprehensive analysis of the conductivity of armchair GNRs using tight-binding methods for use in terahertz antennas concluding that patch antennas implemented using GNRs are suitable for operating at lower frequency range compared to similar metal-patch nano antenna structures [9]. On the other hand, the hexagonal two-dimensional crystal of silicon is called as silicene which also have various applications in electronics with proven stability for use in various areas [11]. The advantage of silicene stems from the expertise on silicon processing technology. Silicene also has a hexagonal lattice configuration but with a buckled structure against the planar configuration of graphene leading to interesting properties such as controlled conductivity with an applied electric field [12]. Similar to GNRs, the thin strips of silicene are called as silicene nanoribbons (SiNRs) which

can be implemented in a wide range of widths [13]. Recently, the optical response of thin SiNRs are measured which show a highly frequency-dependent characteristics as in GNRs [14].

As it is summarized above, there are numerous studies regarding the calculation of the dielectric function of GNRs and SiNRs with various approaches. However, a study comparing the terahertz and optical characteristics of equivalent GNR and SiNR samples and their application as nanostrip transmission lines does not exist in the literature. Evaluation of the transmission line characteristics of GNRs and SiNRs are of importance since nano-sized high-efficiency antennas have feeds which are nanoribbon structures. Apart from the signal transmission to antennas, nano-sized mixers and other components will also obviously need GNR, SiNR or other types of nanoribbons for signal transmission. Hence, GNR and SiNR nanostrip lines have to be modelled accurately. The frequency dependence of the conductivities and dielectric constants of nanostrip lines have to be obtained.

In this work, frequency-dependent complex dielectric functions of realistic equivalent GNR and SiNR samples are obtained utilizing accurate quantum mechanical simulations. Then, the frequency-dependent 3-dimensional and 2-dimensional complex conductivities of these samples are calculated and compared. Next, their transverse electric (TE) and transverse magnetic (TM) SPP wave propagation frequency ranges are discussed. In addition, the frequency-dependent conductivities of the considered samples are imported into a full-wave electromagnetic simulator. GNR and SiNR nanostrip transmission lines are then simulated in terahertz range in order to compare their transmission behaviour for possible use as nanostrip transmission lines.

2. Material and methods

2.1 Quantum mechanical simulations of nanomaterials

Electronic and physical parameters of nano structures can be obtained utilizing various methods such as tight-binding and first-principles simulations. There are various methods for first-principles calculations where DFT is the prominent method thanks to its proven accuracy by solving Kohn-Sham equations with appropriate exchange-correlation functionals [15]. Basically, DFT produces electron density matrix from which various properties such as conductance, transmission or dielectric function can be extracted. As mentioned before, DFT is also used for the investigation of graphene and silicene structures giving accurate results. In this study, a commercial DFT package, Atomistix Toolkit (ATK®) from Quantumwise AS is utilized for the simulation of the considered samples [16]. After obtaining the electron density, Kubo-Greenwood formalism is used for calculating the frequency-dependent complex dielectric function in ATK® [17]. On the other hand, after obtaining the complex conductivities of GNR and SiNR samples, these data are imported into XFDTD® full-wave electromagnetic simulation tool [18] for obtaining transmission characteristics of GNR and SiNR nanostrip lines.

2.2 Considered GNR and SiNR samples

The GNR and SiNR samples considered in this study are armchair nanoribbons with N=20 atoms along the width. The reason of selecting armchair type is that they support long propagation of SPP waves [9]. The unit cells of the GNR and SiNR samples are shown in Fig. 1. Edges of the GNR and SiNR samples are passivated by hydrogen to avoid dangling bonds as a realistic case. The atomic coordinates are optimized in ATK® before the actual calculations using the following parameters: electron temperature is 300K, k-point sampling is (1,20,20), mesh cut-off energy is 250 Ry and the exchange-correlation functional is generalized gradient approximation (GGA). The geometries of the considered samples are optimized until a maximum of 0.02 eV/Å force is achieved on atoms. It is worth noting that after the optimization step, SiNR configuration shows a buckling of 0.47 Å compliant with the literature data [19].

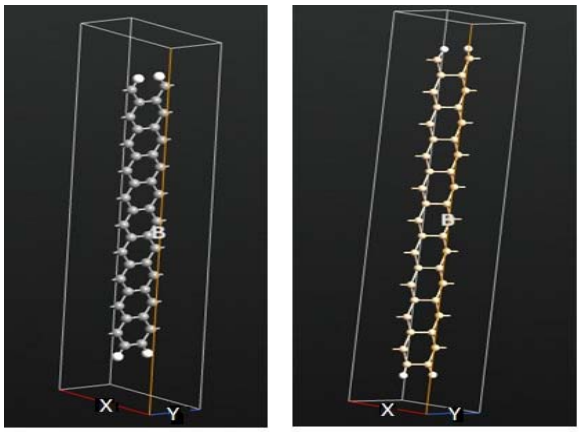

Fig. 1. Considered GNR (a) and SiNR (b) samples

2.3. Calculation of the conductivities from the dielectric function

Since the quantum mechanical simulation tools generally output the dielectric or susceptibility tensor, two- and three-dimensional conductivities should be computed from these quantities. The relation between the three-dimensional bulk conductivity, $\sigma_{3D}(\omega)$, and the susceptibility tensor, $\chi(\omega)$, can be given as in Equation 1 where ω is the angular frequency [20].

$$\sigma_{3D}(\omega) = -i.\omega.\chi(\omega) \quad (1)$$

Similarly, two-dimensional conductivity is calculated using Equation 2 where d is the thickness of the sample [21].

$$\sigma_{2D}(\omega) = \sigma_{3D}(\omega).d \quad (2)$$

It is worth noting that since the susceptibilities are obtained as a function of frequency in ATK®, Equations 1 and 2 can be evaluated easily by exporting the susceptibility data into any mathematical tool.

3. Results and discussion

The actual DFT simulations are performed with a double-polarized basis set after the geometric optimization step. Kubo-Greenwood formalism is utilized for extracting the dielectric function in ATK® with a broadening of 0.5 eV and four contributing bands for 10001 energy points. The frequency-dependent complex dielectric functions of the GNR and SiNR samples in the electron transport direction (y-direction) are obtained in ATK® for the frequency range of 0-10^{15} Hz as shown in Figs. 2 and 3, respectively. The order of magnitudes of the obtained dielectric functions are in consistency with the previous studies for both GNR [10] and SiNR samples [22].

After verifying that the computed dielectric functions are compatible with the literature, the susceptibility tensor of the samples are exported from ATK® into Scilab® environment for calculating the complex conductivities as explained in subsection 2.3. Obtained frequency-dependent three-dimensional conductivities of the GNR and SiNR samples are shown in Fig. 4 and Fig. 5, respectively, for the transport direction. It is worth emphasizing that the conductivities in Fig. 4 and Fig. 5 are bulk conductivities. From a conductivity point of view, it can be stated that both the GNR and the SiNR samples show high conductance behaviour in the range of approximately 70THz-300THz and 92THz-450THz range, respectively, if the high conductance is taken as the range where the conductance lies in the 3dB margin of its maximum value. It is worth noting that the considered samples can be utilized as nanostrip transmission lines at also lower and upper frequencies however losses would be higher.

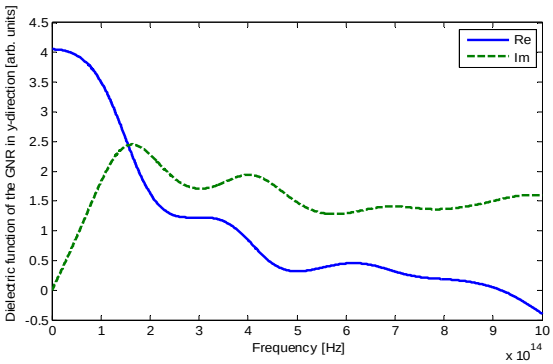

Fig. 2. Frequency-dependent complex dielectric function of the GNR sample in the transmission direction

In order to make a comparison with the conductivity data calculated using other methods in the literature, the two-dimensional sheet conductivities, $\sigma_{2D}(\omega)$, of the samples are calculated using Eq. 2 by taking the thicknesses of the GNR and SiNR samples as 0.34 nm and 0.44 nm, respectively [23, 24].

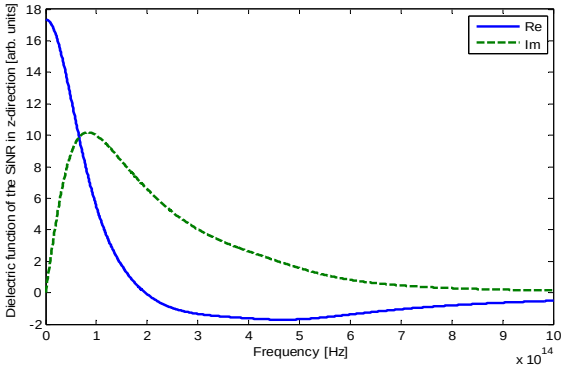

Fig. 3. Frequency-dependent complex dielectric function of the SiNR sample in the transmission direction

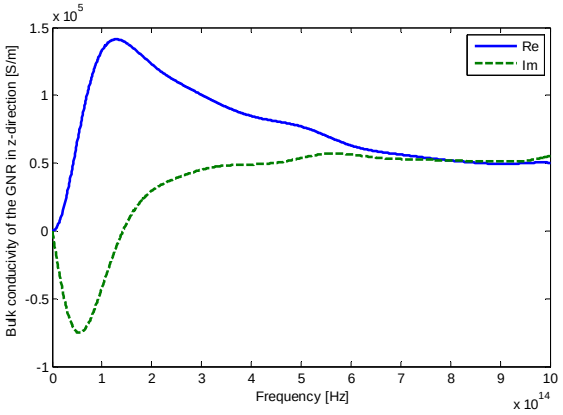

Fig. 4. Frequency-dependent bulk conductivity of the GNR sample in the transmission direction

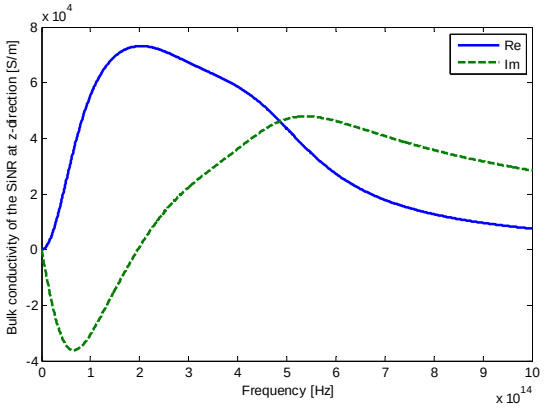

Fig.5. Frequency-dependent bulk conductivity of the SiNR sample in the transmission direction

Calculated frequency-dependent sheet conductivities are given in Fig. 6 and Fig. 7, respectively for the GNR and SiNR samples. It is worth noting that the sheet conductivities of Fig. 6 and Fig. 7 are normalized to conductance quantum (G_Q) which has a value of 7.748x10^{-5} S [2]. It is worth noting that the order of the obtained sheet conductivity of the GNR sample is compliant with the tight-binding calculation results in the literature [9]. However one of the novelties of this study is that the

conductivities of equivalent GNR and SiNR samples are obtained up to 1000 THz using first-principles approach. Moreover, as it is clear from Figs. 6 and 7 that SiNR exhibits a similar but lower conductivity than the equivalent GNR. It is worth noting that the obtained conductivities are on the order of conductance quantum and show little ripples as also expected by theoretical calculations given in [9] for thin nanoribbons.

It is also important to compare the SPP wave transmission characteristics of GNR and SiNR patches. In [9], it is shown that TM mode SPP waves exist in nanoribbon patch structures at frequencies where the imaginary part of the conductance in the transport direction (Im{σ_{zz}}) is positive. Similarly TE mode SPP waves can propagate in these structures if Im{σ_{zz}}<0. Taking these conclusions into consideration, it can be seen from Fig. 6 that the considered GNR sample would permit TE SPP waves in the frequency range of 0-141 THz and TM SPP waves for 141-1000 THz. Similarly, from Fig. 7, SiNR propagates TE SPP waves for 0-198 THz and TM SPP waves for 198-1000 THz range. Considering that TM SPP waves have longer propagation lengths [9], it can be stated that the GNR sample is advantageous for use in SPP wave propagation with a wider TM SPP frequency range compared to its SiNR equivalent.

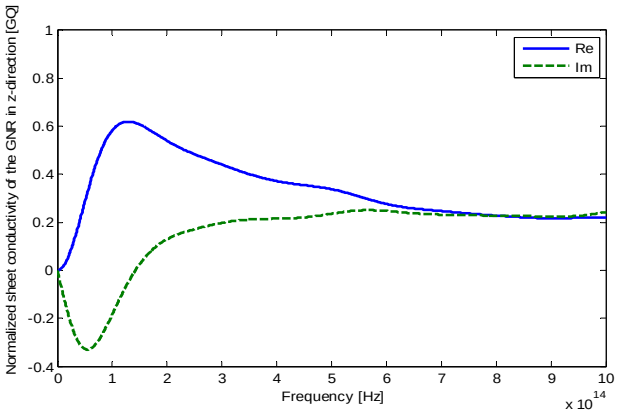

Fig. 6. Frequency-dependent normalized sheet conductivity of the GNR sample in the transmission direction

In order to fully evaluate the differences of utilizing GNR and SiNR as nanostrip lines, obtained

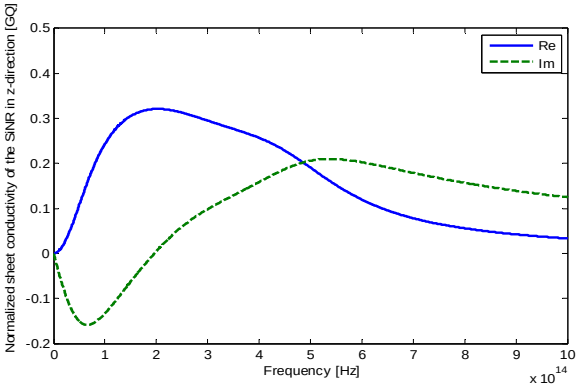

Fig. 7. Frequency-dependent normalized sheet conductivity of the SiNR sample in the transmission direction

anisotropic frequency-dependent conductivities are imported into the full-wave electromagnetic simulation tool XFDTD® 7 [18]. The GNR and SiNR samples are configured as nanostrip lines as shown in Fig. 8. The nanostrip lines are simulated using SiO_2 substrate with $\varepsilon_r = 12.9$, thickness of 10 μm and perfect electrical conductor at the ground plane with air above the structure. These sample parameters and the frequency range are selected for testing the appropriateness of the GNR and SiNR nanostrip samples for terahertz nano antenna applications [9]. Obtained transmission characteristics are shown in Fig. 9 for both GNR and SiNR lines. As it can be seen from these plots, the loss of the GNR sample is lower than its SiNR counterpart due to its higher conductivity. This sample simulation demonstrates that due to their higher conductivity, GNRs can be advantageous over their SiNR counterparts from the signal transmission viewpoint. It can be concluded that the origin of the higher conductivity of GNR on SiNR is mainly due to the planar structure of GNR enabling lower elastic scattering in atomic sites.

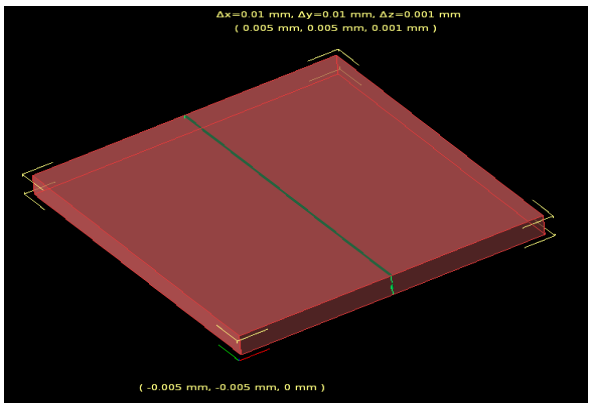

Fig. 8. Geometry of the GNR and SiNR nanostrip line (green line → nanostrip line and perfect electrical conductor at the bottom ground plane)

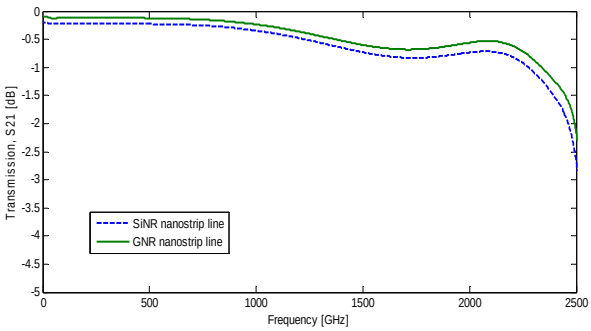

Fig. 9. Transmission characteristics of equivalent GNR and SiNR samples for the terahertz band obtained from XFDTD®

In summary, it is shown that the GNR sample permits wider frequency range for the propagation of TM SPP waves compared to its SiNR counterpart. In addition, it is also exposed that armchair GNR sample seems to be more appropriate than its equivalent armchair SiNR for

implementing nanostrip transmission lines due to its higher conductivity as it can be seen from Figs. 6 and 7, respectively. Hence, it can be stated that the GNR sample has advantageous characteristics for having both wider TM SPP wave propagation frequency range and higher conductivity than its equivalent SiNR sample.

4. Conclusions

Complex dielectric functions, complex conductivities and SPP wave propagation properties of realistic equivalent GNR and SiNR samples in terahertz and optical band are investigated and compared in this study. The novel points of this study are: i) frequency-dependent complex dielectric functions of equivalent realistic armchair GNR and SiNR samples are obtained for comparison utilizing DFT approach combined with Kubo-Greenwood formalism, ii) frequency-dependent complex bulk and sheet conductivities of equivalent GNR and SiNR samples are calculated and compared, iii) the complex conductivity of an armchair SiNR is obtained using ab initio methods for the first time in the literature, iv) TE and TM SPP wave propagation characteristics of the GNR and SiNR samples are compared, and v) practical nanostrip lines of the GNR and SiNR samples are simulated with FDTD method in terahertz band using the frequency-dependent conductivity data imported from accurate quantum mechanical simulations. From the obtained characteristics, it is concluded that the GNR sample is more advantageous than its equivalent SiNR counterpart for having wider TM SPP transmission characteristics and higher conductivity.

Acknowledgement

The author would like to thank Remcom Inc. and Atomistix A/S for their valuable support.

References

[1] K. F. Mak, M. Y. Sfeir, Y. Wu, C. H. Lui, J. A. Misewich, T.F. Heinz, Phys. Rev. Lett. **101**, 196405 (2008).
[2] M-Y. Han, B. Ozyilmaz, Y. Zhang, P. Kim, Phys. Rev. Lett. **98**, 206805 (2007).
[3] G. R. Hotopan, S. Ver-Hoeye, C. Vazquez-Antuna, R. Camblor-Diaz, M. Fernandez-Garcia, F. Las Heras Andres, P. Alvarez, R. Menéndez, Prog. Electr. Res. **118**, 57 (2011).
[4] R. Hambach, PhD Thesis, Ecole Polytechnique, (2010).
[5] P. Rani, G.S. Dubey, V.K. Jindal, Phys. E: Low-dim. Sys. Nano. **62**, 28-35 (2014).
[6] A.G. Marinopoulos, L. Reining, A. Rubio, V. Olevano, Phys. Rev. B, **69**, 245419 (2004).
[7] J. Goschniak, D.T.H. Tan, Sci. Rep. **3**, 1 (2013).
[8] J.E. Burke, Analytical study of tunable bilayered graphene dipole antenna, Development and Engineering Center Report, New Jersey (2011).
[9] J.M. Jornet, I.F. Akyildiz, IEEE J. Sel. Area. Comm./Supp., **31**, 685-694 (2013).
[10] R. Denk, M. Hohage, P.Zeppenfeld, J. Cai, C.A. Pignedoli, H. Söde, R. Fasel, X. Feng, K. Müllen, S. Wang, D. Prezzi, A. Ferretti, A. Ruini, E. Molinari, P. Ruffieux, Nat. Comm. **5**, 4253 (2014).
[11] P. dePadova, C. Ottaviani, C. Quaresma, B. Olivieri, P. Imperatori, E. Salomon, T. Angot, C. Quagliano, C. Romano, A. Vona, 2D Mat., **1**, 021003 (2014).
[12] M. Houssa, M. van den Broek, E. Scalise, G. Pourtios, V.V. Afanasev, A. Stesmans, Phys. Chem. Chem. Phys. **15**, 3702 (2013).
[13] S. Trivedi, A. Srivastava, R. Kurchania, J. Comp. Theo. Nano. **11**, 789 (2014).
[14] Y. Borensztein, G. Prévot, L. Masson, Phys. Rev. B. **89**, 245410 (2014).
[15] J.M. Soler, E. Artacho, J.D. Gale, A. García, J. Junquera, P. Ordejón, D. Sánchez-Portal, J. Phys.: Cond. Mat. **14**, 2745 (2002).
[16] Atomistix ToolKit, QuantumWise A/S, Copehnagen (2014).
[17] W.A. Harrison, Solid State Theory, McGraw-Hill Press, New York (1970).
[18] XFDTD version 7.4, Remcom Inc., State College, PA (2014).
[19] S. Cahangirov, M. Topsakal, E. Akturk, H. Sahin, S. Ciraci, Phys. Rev. Lett **102**, 236804 (2009).
[20] R.M. Martin, Electronic Structure, Cambridge University Press, Cambridge (2004).
[21] M. D'Amore, A.G. D'Aloria, M.S. Sarto, Int. Conf. Electr. Comp. Gothenburg, 482 (2014).
[22] B. Mohan, A. Kumar, P.K. Akuwalia, Phys. E: Low-dim. Sys. Nano. **61**, 40 (2014).
[23] X. Zhou, X. Ling, H. Luo, S. Wen, App. Phys. Lett. **101**, 251602 (2012).
[24] S.S. Batsanov, Inorg. Mat. **37**, 871 (2001).

*Corresponding author: syamacli@gmail.com